RSC Advances

This is an *Accepted Manuscript*, which has been through the Royal Society of Chemistry peer review process and has been accepted for publication.

Accepted Manuscripts are published online shortly after acceptance, before technical editing, formatting and proof reading. Using this free service, authors can make their results available to the community, in citable form, before we publish the edited article. This *Accepted Manuscript* will be replaced by the edited, formatted and paginated article as soon as this is available.

You can find more information about *Accepted Manuscripts* in the Information for Authors.

Please note that technical editing may introduce minor changes to the text and/or graphics, which may alter content. The journal's standard Terms & Conditions and the Ethical guidelines still apply. In no event shall the Royal Society of Chemistry be held responsible for any errors or omissions in this *Accepted Manuscript* or any consequences arising from the use of any information it contains.

ROYAL SOCIETY OF CHEMISTRY

www.rsc.org/advances

Synthesis, characterization, TDDFT calculation and biological activity of tetradentate ligand based square pyramidal Cu(II) complexes

Apurba Bhunia,[a] Soumen Manna,[a] Soumen Mistri,[a] Aparup Paul,[a] Rajesh Kumar Manne,[b] Manas Kumar Santra,[b] Valerio Bertolasi,[c] Subal Chandra Manna*,[a]

[a]*Department of Chemistry and Chemical Technology, Vidyasagar University, Midnapore 721102, West Bengal, India, E-mail: scmanna@mail.vidyasagar.ac.in, Fax: (91) (03222) 275329.*

[b] *National Centre for Cell Science, NCCS Complex, Pune University Campus Ganeshkhind, Pune-411 007, Maharashtra, India.*

[c]*Dipartimento di Scienze Chimiche e Farmaceutiche, Centro di Strutturistica Diffrattometrica, Università di Ferrara, Via L. Borsari, 46, 44100 Ferrara, Italy.*

Distorted square pyramidal complexes $[Cu(L^1)(H_2O)]\cdot ClO_4$ (**1**), $[Cu(L^2)(H_2O)]\cdot ClO_4$ (**2**) and $[Cu(L^3)(H_2O)]\cdot ClO_4$ (**3**) (HL^1 = *o*-{[2-(2-aminoethylamino)ethylimino]methyl}phenol; HL^2 = 2-{[2-(2-aminoethylamino)ethylimino]methyl}-6-methoxyphenol; HL^3= *o*-{1-[2-(2-aminoethylamino)ethylimino]ethyl}phenol) have been synthesized, and characterized by X-ray crystallography and spectroscopic analysis. All the complexes exhibit fluorescence at room temperature [λ_{ex} = 267 nm, λ_{em} = 312, 329 and 357 nm, φ = 0.52 for **1**; λ_{ex} =272 nm, λ_{em} = 312, 329 and 355 nm, φ = 0.46 for **2**; λ_{ex} = 265 nm, λ_{em} = 312, 356 and 377 nm, φ = 0.33 for **3**]. The electronic structure and photophysical properties of the ligands and complexes were calculated by density functional theory (DFT) and time-dependent density functional theory (TD-DFT) methods using the B3LYP, B3PW91 and MPW1PW91 functionals, with 6-31G (d-p) and LanL2DZ basis sets. The results of TD-DFT calculations are functional-dependent and among the functionals, B3LYP was able to best reproduce the experimental results. Catecholase activity of **1**-**3** has been investigated using 3,5-di-tert butyl catechol (3,5-DTBC) as model substrate and found that complexes are active for catalyzing aerobic oxidation of 3,5-DTBC to 3,5-di-tert butyl

RSC Advances Accepted Manuscript

benzoquinone (3,5-DTBQ). The compound with more distorted square pyramidal geometry shows higher rate of catalytic activity. All the complexes have been tested for their anticancer activities in human breast (MCF7) cancer cell lines. Complexes show dose dependent suppression of cell viability with IC_{50} values 30, 68 and >100 μM for **1**, **2** and **3**, respectively. Anticancer activities of **1-3** and cisplatin were compared, and found that **1-3** were relatively less active than cisplatin.

Introduction

Coordination compounds of Cu(ll) using chelating ligands are of immense interest in the area of catalysis,[1] fluorescence,[2] chemical sensors,[3] etc. Cu(ll) complexes are less toxic and have important cellular effect such as neurotransmission, cellular respiration, etc.[4] On the other hand, Cu(ll) compounds exhibit interesting anticancer activity[5] and show catecholase activity.[6] These coordination compounds are generally synthesized[7] by adopting self-assembly techniques and depending on chelating ligands, Cu(ll) exhibit several coordination geometries.[8] Adjustment of reaction conditions, which control the metal-ligand aggregation process, is also a vital factor in designing and synthesizing of Cu(ll) compound.

Quantum chemical calculation using density functional theory (DFT) and time dependent density functional theory (TD-DFT)[9] have been widely used to study the structural, electronic and spectroscopic properties of different compounds. The results of DFT/TD-DFT computation depends on the choice of different DFT functionals.[10] It is to note that the use of DFT/TD-DFT computation to explore the electronic properties of Cu(ll) compounds are less documented in the literature.[11]

RSC Advances Accepted Manuscript

Over the last few years we have been actively engaged in designing and synthesis of Cu(ll) coordination compounds. Here we have chosen tetradentate (O,N,N,N donor) Schiff bases *o*-{[2-(2-aminoethylamino)ethylimino]methyl}phenol (HL^1), 2-{[2-(2-aminoethylamino)ethylimino]methyl}-6-methoxyphenol (HL^2) and *o*-{1-[2-(2-aminoethylamino)ethylimino]ethyl}phenol (HL^3), and synthesized $[Cu(L^1)(H_2O)]\cdot ClO_4$ (**1**), $[Cu(L^2)(H_2O)]\cdot ClO_4$ (**2**) and $[Cu(L^3)(H_2O)]\cdot ClO_4$ (**3**). The IR and electronic spectral properties of the ligands and complexes were explained by DFT/TD-DFT computation using different functionals. Anticancer activities in human breast (MCF7) cancer cell and catecholase activities of complexes have been investigated.

Experimental

Materials. High purity diethylenetriamine (Aldrich), 2-hydroxybenzaldehyde, 2-hydroxy-3-methoxybenzaldehyde and 2′-hydroxyacetophenone (Spectrochem - India) were purchased and used as received. All other chemicals used were of analytical grade. Solvents used for spectroscopic studies were purifies and dried by standard procedures before use.[12]

Physical measurements. Elemental analyses (carbon, hydrogen and nitrogen) were performed using a Perkin-Elmer 240C elemental analyzer. IR spectra were recorded as KBr pellets on a Bruker Vector 22 FT IR spectrophotometer operating from 400 to 4000 cm^{-1}. ESI-MS spectra were recorded on a JEOL MS 700 mass spectrometer in fast atom bombardment (FAB) mode. NMR spectra of ligands recorded on Bruker 200 MHz instrument. Electronic absorption spectra were obtained with Shimadzu UV-1601 UV-vis spectrophotometer at room temperature. Quartz

RSC Advances Accepted Manuscript

cuvettes with a 1 cm path length and a 3 cm^3 volume were used for all measurements. Emission spectra were recorded on a Hitachi F-7000 spectrofluorimeter. Room temperature (300 K) spectra were obtained in methanol solution using a quartz cell of 1 cm path length. The slit width was 2.5 nm for both excitation and emission.

The fluorescence quantum yield was determined using phenol as a reference and water [refractive index (η), 1.333)] medium for phenol. The solvent used for complexes is methanol (η, 1.329). Emission spectra were recorded by exciting the complex and the reference phenol at the same wavelength, maintaining nearly equal absorbance (~0.1). The area of the emission spectrum was integrated using the software available in the instrument and the quantum yield was calculated[13] according to the following equation:

$$\Phi_S = \Phi_r \frac{A_S}{A_r} \frac{I_r}{I_S} \frac{\eta_S^2}{\eta_r^2}$$

Where Φ_s and Φ_r are the fluorescence quantum yield of the sample and reference, respectively. A_s and A_r are the respective optical densities at the wavelength of excitation, I_s and I_r correspond to the areas under the fluorescence curve; and η_s and η_r are the refractive index values for the sample and reference, respectively.

Synthesis of the ligands

The ligands *o*-{[2-(2-aminoethylamino)ethylimino]methyl}phenol (HL^1), 2-{[2-(2-aminoethylamino)ethylimino]methyl}-6-methoxyphenol (HL^2) and *o*-{1-[2-(2-aminoethylamino)ethylimino]ethyl}phenol (HL^3) were prepared by condensation reaction of diethylenetriamine and related aldehydes / ketones. Details of synthesis and characterization of ligands are given in supporting information. ^1H NMR spectra of HL^1, HL^2 and HL^3 in $CDCl_3$ is shown in Fig. 1.

RSC Advances Accepted Manuscript

Synthesis of complexes

Caution! Perchlorate salts of metal complexes with organic ligands are potentially explosive. Only a small amount of material should be prepared, and it should be handled with care.

The complexes have been synthesized by adopting the procedures schematically given in Scheme 1.

Scheme 1. Synthesis of **1**, **2** and **3**

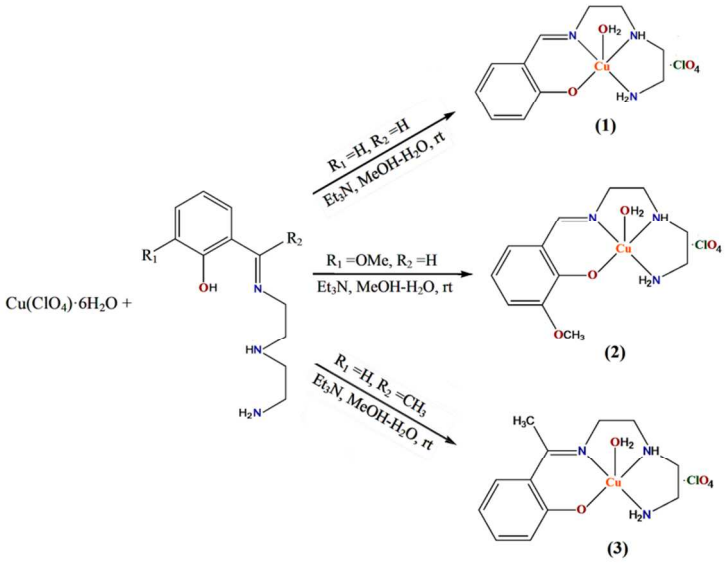

Synthesis of $[Cu(L^1)(H_2O)]\cdot(ClO_4)$ (1). A methanolic solution (5 mL) of triethylamine (1 mmol, 0.10 g) was added dropwise to a methanolic solution (10 mL) of HL^1 (1 mmol, 0.20 g) with constant stirring for 5 min. To this resulting mixture, dropwise addition of methanolic solution (10 mL) of copper perchlorate hexahydrate (1 mmol; 0.370 g) yielding a reddish brown solution. The whole reaction mixture was stirred for 2 hours and filtered. Blue single crystals suitable for X-ray diffraction quality were obtained after a few days on keeping the solution in a refrigerator. Yield 0.302 g (78 %). $C_{11}H_{18}CuN_3O_6Cl$ (387.27): C, 34.11; H, 4.68; N, 10.84 %.

RSC Advances Accepted Manuscript

Found: C, 34.09; H, 4.65; N, 10.85 (%). IR (cm^{-1}): 3200-3500 (br,vs), 3102 (s), 2972 (s), 2943 (s), 1649 (s), 1561 (vs), 1460 (s), 1418 (s), 1372 (s), 1300 (s), 1115 (s), 1072 (s), 818 (w), 782 (w), 670 (w), 561 (s), 515 (s).

Synthesis of $[Cu(L^2)(H_2O)]\cdot(ClO_4)$ (2) and $[Cu(L^3)(H_2O)]\cdot(ClO_4)$ (3). These complexes were synthesized by following the same procedure as adopted for complex **1**, using HL^2 (1 mmol, 0.24 g) and HL^3 (1 mmol, 0.22 g) for **2** and **3**, respectively, instead of HL^1. For **2**: Yield 0.333 g (80 %). $C_{12}H_{20}CuN_3O_7Cl$ (417.30): C, 34.53; H, 4.83; N, 10.06 %. Found: C, 34.52; H, 4.85; N, 10.07 (%). IR (cm^{-1}): 3200-3500 (br,vs), 2975 (s), 2943 (s), 1639 (vs), 1558 (vs), 1467 (s), 1418 (vs), 1372 (s), 1297 (s), 1124 (w), 1079 (s), 883 (w), 815 (w), 782 (w), 629 (s), 515 (s). For **3**: Yield 0.305 g (76 %). $C_{12}H_{20}CuN_3O_6Cl$ (401.30): C, 35.88; H, 5.02; N, 10.46 %. Found: C, 35.87; H, 5.00; N, 10.49 (%). IR (cm^{-1}): 3200-3500 (br,vs), 3094 (s), 2982 (s), 2943 (s), 1643 (vs), 1561 (vs), 1467 (vs), 1414 (vs), 1372 (s), 1300 (s), 1124 (s), 1108 (s), 1082 (s), 883 (w), 779 (s), 639 (s), 551 (s).

Crystallographic data collection and refinement.

Data collection of complexes **1**, **2** and **3** were carried out by using a Nonius Kappa CCD diffractometer with graphite monochromated Mo-Kα radiation, at room temperature. The data sets were integrated with the Denzo-SMN package[14] and corrected for Lorentz, polarization and absorption effects (SORTAV).[15] The structures were solved by direct methods using SIR97[16] system of programs and refined using full-matrix least-squares with all non-hydrogen atoms anisotropically and hydrogens included on calculated positions, riding on their carrier atoms**.** All calculations were performed using SHELXL-97[17] and PARST[18] implemented in WINGX[19] system of programs. Graphical programs used are those included in the WinGX System,[19] and Diamond.[20] Crystal data and details of refinements are given in Table 1. CCDC 1060158 -

RSC Advances Accepted Manuscript

1060160 contain the supplementary crystallographic data for this article and are deposited at the Cambridge Crystallographic Data Centre (CCDC).

Theory and computational methods

All computations were performed using the Gaussian 09 (G09) software package,[21] by using the Becke's three-parameter hybrid exchange functional and the Lee-Yang-Parr non-local correlation functional (B3LYP),[10a] Becke's three-parameter Perdew-Wang 1991 functional (B3PW91),[10b] and Barone's Modified Perdew-Wang 1991 exchange functional and Perdew and Wang's 1991 correlation functional (MPW1PW91)[10c]. In the calculation 6-31G (d-p) basis set was assigned to all elements with the exception of copper, for which the Los Alamos effective core potentials plus the Double Zeta (LanL2DZ)[22] basis set were employed. The geometric structures of the complexes in the ground state (doublet) were fully optimized at the B3LYP, B3PW91 and MPW1PW91 levels. The vibration frequency calculations were performed to ensure that the optimized geometries represent local minima associated with positive eigen values only.

For the purpose of comparison of ground state (S_0) stability of keto and enol tautomeric forms of the ligands, potential energy scan were performed indicating the reaction coordinates corresponding to the change of location of the proton from N_{donor} to $O_{acceptor}$. During potential energy scan all other degrees of freedom were remain undisturbed without imposing any symmetry limit for the ground S_0 state. [23]

Vertical electronic excitations based on B3LYP, B3PW91 and MPW1PW91 functionals were obtained with the time-dependent density functional theory (TD-DFT) formalism[24] in methanol using the conductor-like polarizable continuum model (CPCM).[25] GaussSum[26] was used to calculate the fractional contributions of various groups to each molecular orbital.

RSC Advances Accepted Manuscript

Calculated coordination geometries of methanol solvated complexes are shown in Tables 2 and 1S.

Cell culture

Breast cancer cell line MCF7 was cultured in DMEM medium as monolayers supplemented with 10 % FBS, 100U/ml penicillin and 100 µg/ml streptomycin at 37°C in a humid condition with 5% CO_2 atmosphere.

In *vitro* cytotoxicity assay

The cytotoxicity of the compounds was determined by the MTT (3-(4, 5 dimethylthiazol-2-yl)-2-5 diphenyltetrazolium bromide) assay. Cells were seeded at 5 x 10^3 cells per well in 96-well plates. Next day, cells were treated with different concentrations (0.01 – 100 µM) of the compounds for 48 hour. Then, MTT solution was added to each well and further incubated for 3.5 h at 37°C in a humid, 5% CO_2 atmosphere. Finally, medium containing MTT solution was replaced by MTT solvent (4 mM HCl and 0.1% Triton X-100) and incubated for 15 minute at room temperature. The absorbance was read in Thermo Pierce Elisa plate reader at 570 nm. The percentage of growth inhibition was calculated with respected to vehicle (DMSO) treated cells. All the experiments were repeated for three times.

Results and discussion

Crystal structure description

$[Cu(L^1)(H_2O)]\cdot(ClO_4)$ (**1**), $[Cu(L^2)(H_2O)]\cdot(ClO_4)$ (**2**) and $[Cu(L^3)(H_2O)]\cdot(ClO_4)$ (**3**). X-ray structural analysis of complexes **1-3** revealed that the crystals comprise almost identical mononuclear cationic species and Ortep[27] views of these complexes are shown in Figs. 2, 1S, 2S.

RSC Advances Accepted Manuscript

In each case, the complex is counter balanced by perchlorate anion. The metal has a five coordinate distorted square pyramidal coordination environment where three nitrogen and one oxygen donor from chelating Schiff base form the basal plane, while an aqua ligand occupy the apical position. In the basal plane the coordination bond distances fall in a ranges 1.922(2)-2.010(3) Å (for **1**), 1.908(3)- 2.029(4) Å (for **2**), 1.862(3)- 2.029(4) Å (for **3**), while the apical Cu(1)-O(2) bond is significantly longer [2.394(2) Å (for **1**); 2.428(3) Å (for **2**); 2.465(3) Å (for **3**)] (Table 2). For all complexes, Cu(1)-$O(2)_{water}$ and Cu(1)-$O(1)_{phenolic}$ bond distances are largest and smallest bond distances, respectively. The largest bond angle in all the complexes is O(1)-Cu(1)-N(2) [172.9(1)°, 178.26(14)°, 176.8(2)°], whereas smallest bond angle in **1** and **2** is N(1)-Cu(1)-N(2) [84.6 (1)°, 84.8(2)°], and in **3** is N(2)-Cu(1)-N(3) [79.5(2)°].

Hydrogen bonding interactions (Table 2S) results the formation of supramolecular dimer for **1** (Fig. 3) and **3** (Fig. 5), and supramolecular trimer for **2** (Fig. 4). $R^2_2(8)$ H-bonding synthons[28] [Figs. 3S, 4S, 5S] between phenolic oxygen (O1) and coordinated water helps the formation of supramolecular dimeric structure of all the complexes. Additional $R^2_1(5)$ supramolecular synthon [formed among methoxy oxygen (O7), phenoxy oxygen (O1) and amine (N3) hydrogen] in **2** produces spramolecular trimeric unit of **2** (Fig. 4). Finally, C-H···π interactions[29] [Table 3S; C(9)-H(9A)···C_g(4), 2.73 Å for **1**; C(9)-H(9A)···C_g(4), 2.64 Å for **2**; C(8)-H(8A)···C_g(4), 3.14 Å and C(10)-H(10A)···C_g(4), 2.76 Å for **3**] favor the formation of 2D networks of **1** (Fig. 6S) and **3** (Fig. 7S), whereas 1D chain of **2** (Fig. 8S).

We have calculated Puckering parameters[30] for detail study of ring conformations of complexes. Conformations of ring 1 (Cu1,N1,C8,C9,N2) and ring 2 (Cu1,N2,C10,C11,N3) are given in the Table 3. Ring 1 is envelope (E_4) in complex **1**, whereas twisted/envelope in complex **2** ($^5T_4/E_4$) and complex **3** ($^3T_4/E_4$). On the other hand ring 2 possesss twisted/envelope

RSC Advances Accepted Manuscript

conformation in complex **1** ($^4T_3/E_3$) and complex **2** ($^4T_3/^4E$), but envelope (E_3) in complex **3**. In all complexes phase angle (φ_2) values are positive for ring 1 and negative in ring 2 i.e. specular. Two structures with same cationic unit as in **1** were reported by Zhu *et al* [31a] and Cusmano *et al* [31b]. Comparison of structural parameters (Table 4S) of reported compounds with **1** reveals that coordination geometry of Cu in **1** is more close to ideal square pyramidal than reported compounds.

Geometrical optimization and electronic structure

DFT and TD-DFT computations of optimized structures of ligands [HL^1, HL^2, HL^3] and complexes **1-3** were performed to establish their electronic structure and spectral transitions. The geometric structures of the isolated ligands and complexes **1-3** (excluding perchlorate anion) were fully optimized at the Becke's three-parameter hybrid exchange functional and the Lee-Yang-Parr non-local correlation functional (B3LYP) level in the ground state (singlet for ligands and doublet for complexes **1-3**). The optimized structures of ligands are shown in Fig. 9S. The potential energy scan of the ligands in the singlet ground state shows that the keto-tautomeric forms (Chart 1S, supporting information) were more stable by an amount of energy of 5.02 and 0.628 kcal mol^{-1}, for HL^1 and HL^2, respectively, than the corresponding enol form (Figs. 6 and 10S). On the other hand for HL^3, both keto and enol-tautomeric forms have comparable stability (Fig. 11S).

The optimized structures of complexes **1-3** along with their Mulliken charge distribution are depicted in Figs. 12S-14S. The comparison of bond lengths and angles between calculated and X-ray structure shows an ample agreement (Tables 2 and 1S). The orbital diagram along with their energies and contributions from the ligands and metal are given in Fig. 15S, and a correlation of MOs are given in Figs. 16S and 17S. For **1**, the energies of highest occupied

RSC Advances Accepted Manuscript

molecular orbital (HOMO) and lowest unoccupied molecular orbital (LUMO) are – 5.97 eV and - 1.96 eV, respectively. For **2**, energies of HOMO and LUMO orbitals are -5.68 eV and -1.92 eV, respectively. Whereas for **3**, the corresponding values are -5.90 eV and -1.85 eV, respectively. As a matter of fact, the HOMO-LUMO energy difference in **3** is larger (ΔE = 4.05 eV) compared to the values of **1** (ΔE = 4.01eV) and **2** (ΔE = 3.76 eV), indicating a lower kinetic stability[32] of **2** with respect to **1** and **3**. Contribution of Schiff base, water and copper to HOMO [97 % L^1, 0 % H_2O, 3 % Cu for **1**; 98 % L^2, 0 % H_2O, 2 % Cu for **2**; 97 % L^3, 0 % H_2O, 3 % Cu for **3**] and LUMO [99 % L^1, 0 % H_2O, 1 % Cu for **1**; 99 % L^2, 0 % H_2O, 1 % Cu for **2**, 99 % L^1, 0 % H_2O, 1 % Cu for **3**] indicate that these orbitals are characterized by the ligand orbitals (≥ 97 %).

TD-DFT calculations in methanol using conductor-like polarizable continuum model (CPCM) were performed and theoretically possible spin-allowed doublet-doublet electronic transitions with their assignment are listed in Tables 4 and 5S. The TD-DFT results show that [HOMO-1 (β) → LUMO + 2 (β); [HOMO-1 (β) → LUMO+3 (β)], HOMO-12 (β) → LUMO (β); HOMO-9 (β) → LUMO (β)] and [HOMO-1 (α) → LUMO+6 (α)] are the possible highest energy electronic transitions, for complexes **1**, **2** and **3** respectively. On the other hand, HOMO-3 (β) → LUMO (β) and HOMO (β) → LUMO (β)] electronic transitions represent possible lowest energy electronic transitions for all the complexes. The highest energy electronic transitions for **1** are $ILCT^{\theta}$ (intra ligand charge transfer in L^1) and $LMCT^{\delta}$ (L^1 to metal charge transfer) in nature, and the lowest energy electronic transitions are IMCT (intra metal charge transfer) and $LMCT^{\delta}$ in nature. For **2**, the highest energy transition is $LMCT^{\Gamma}$ (L^2 to metal charge transfer) and the lowest energy transitions have IMCT and $LMCT^{\Gamma}$ character. Whereas for **3**, the highest

RSC Advances Accepted Manuscript

energy transition is $LMCT^{\Omega}$ (L^3 to metal charge transfer) and the lowest energy transitions are IMCT and $LMCT^{\Omega}$ in nature.

In **1** the experimental electronic transitions (Fig. 7) at 241 nm may be assign to a combination of $ILCT^{\theta}$ [HOMO(α)→ LUMO+1(α)] and $LMCT^{\delta}$ [HOMO-7(β) → LUMO(β)] transitions, and the transition at 361 nm is $ILCT^{\theta}$ [HOMO-1(α) → LUMO (α); HOMO(α) → LUMO (α); HOMO(β) → LUMO+1(β)] in nature. The experimental transition of **2**, at 206 nm (Fig. 18S) assigned as $LMCT^{\Gamma}$ [HOMO-2 (α) → LUMO +1 (α); HOMO-1 (β) → LUMO+2 (β)] and for **3**, transition at 355 nm (Fig. 19S) may be attributed to $ILCT^{\phi}$ (intra ligand charge transfer in L^3) [HOMO-1(α) → LUMO (α)].

The geometric data of complexes **1-3** derived from X-ray experimental and theoretical calculations (Tables 2 and 1S) show a good agreement. The trigonality τ parameter[33] for five-coordinated complexes calculated as (α-β)/60, where α and β are the two largest coordination bond angles. For a regular trigonal bipyramidal structure with D_{3h} symmetry has τ = 1 and for a regular C_{4v} square pyramidal geometry τ = 0. The τ is calculated from experimental X-ray [0.133 for **1**, 0.329 for **2**, and 0.183 for **3**] and theoretical data [0.191 for **1**, 0.196 for **2**, and 0.158 for **3**]. These values indicate a different distortion in the square pyramidal (*SPY*-5) geometries and form these τ values it is clear that structure of **1** is more close to ideal square pyramidal geometry, whereas more deviation from ideal square pyramidal geometry observed in **2**.

We also performed DFT and TD-DFT computations using B3PW91[10b] and MPW1PW91[10c] functionals, and compared the results with the results obtained using B3LYP functional. It is found that B3LYP functional produced structural (Table 1S) and spectroscopic data (Tables 6S

RSC Advances Accepted Manuscript

and 7S) which are more close to experimental results than B3PW91 and MPW1PW91 functionals.

Ligand photophysical study

The spectrum of HL^1 shows (Fig. 20S) significant transitions at 215 nm (ε ~ 28.85 x 10^4 liter $mole^{-1}$ cm^{-1}), 255 nm (ε ~ 13.57 x 10^4 liter $mole^{-1}$ cm^{-1}), 279 nm (ε ~ 4.5 x 10^4 liter $mole^{-1}$ cm^{-1}), 316 nm (ε ~ 4.1 x 10^4 liter $mole^{-1}$ cm^{-1}) and 400 nm (ε ~ 1.7 x 10^4 liter $mole^{-1}$ cm^{-1}). HL^2 shows (Fig. 21S) significant transitions at 207 nm (ε ~ 17.51 x 10^4 liter $mole^{-1}$ cm^{-1}), 220 nm (ε ~ 19.06 x 10^4 liter $mole^{-1}$ cm^{-1}), 263 nm (ε ~ 8.41 x 10^4 liter $mole^{-1}$ cm^{-1}), 296 nm (ε ~ 5.04 x 10^4 liter $mole^{-1}$ cm^{-1}) and 422 nm (ε ~ 1.90 x 10^4 liter $mole^{-1}$ cm^{-1}). On the other hand HL^3 shows (Fig. 22S) transitions at 206 nm (ε ~ 27.81 x 10^4 liter $mole^{-1}$ cm^{-1}), 275 nm (ε ~ 6.69 x 10^4 liter $mole^{-1}$ cm^{-1}), 316 nm (ε ~ 2.63 x 10^4 liter $mole^{-1}$ cm^{-1}) and shows bands at 389 nm (ε ~ 3.66 x 10^4 liter $mole^{-1}$ cm^{-1}). Results of TD-DFT calculations and details of spectral assignments (Tables 8S - 13S) indicate that the electronic transitions are mainly n → π* and/or π → π* in nature.

Electronic absorption spectra of complexes

The electronic absorption spectrum of **1** (Fig. 7) shows significant transitions at 205 nm (ε ~ 13.43 x 10^4 liter $mole^{-1}$ cm^{-1}), nm 224 nm (ε ~ 2.7 x 10^4 liter $mole^{-1}$ cm^{-1}), 241 nm (ε ~ 2.90 x 10^4 liter $mole^{-1}$ cm^{-1}), 249 nm (ε ~ 21.86 x 10^4 liter $mole^{-1}$ cm^{-1}) 267 nm (ε ~ 2.25 x 10^4 liter $mole^{-1}$ cm^{-1}), and 361 nm (ε ~ 7.21 x 10^3 liter $mole^{-1}$ cm^{-1}). Transitions of **2** occur (Fig. 18S) at 206 nm (ε ~ 19.72x 10^3 liter $mole^{-1}$ cm^{-1}), 236 nm (ε ~ 2.73 x 10^4 liter $mole^{-1}$ cm^{-1}), 272 nm (ε ~ 1.63 x 10^4 liter $mole^{-1}$ cm^{-1}) and 375 nm (ε ~ 4.24 x 10^3 liter $mole^{-1}$ cm^{-1}). On the other hand the spectrum of **3** shows significant transitions (Fig. 19S) at 204 nm (ε ~ 2.76 x 10^4 liter $mole^{-1}$ cm^{-1}), 224 nm (ε ~ 2.18 x 10^4 liter $mole^{-1}$ cm^{-1}), 266 nm (ε ~ 1.13 x 10^4 liter $mole^{-1}$ cm^{-1}) and 355 nm

RSC Advances Accepted Manuscript

($\varepsilon \sim 3.12 \times 10^3$ liter mole^{-1} cm^{-1}). Results of TD-DFT calculation along with details of spectral assignments (Tables 4, 5S and 6S) reveal that experimental spectral bands are mainly due to intra ligand charge transfer (ILCT) i.e., $\pi \rightarrow \pi^*$ or $n \rightarrow \pi^*$ transitions. Spectral bands of **2** appear at higher wavelength in compare to bands of **1**, this is due to the presence of electron donating –OMe group which reduces the energy gap among the electronic energy levels. On the other hand spectral bands of **3** appear at shorter wavelength compare to **1** and **2**, this may cause for the presence of $-CH_3$ group which inhibit the conjugation due to steric crowding and results higher energy transitions.

Fluorescent properties of the complexes

Results of the study of luminescence properties (Fig. 8) are summarized in Table 5. Complexes **1-3** exhibit red shifted emission with a large Stokes shift (40-112 nm). On excitation at 267 nm complex **1** exhibits luminescence bands at 312, 329 and 357 nm with a fluorescence quantum yield Φ_s= 0.52. For **2**, λ_{ex}, 272 nm; λ_{em}, 312, 329, 355 nm and Φ_s= 0.46. For **3**, λ_{ex}, 265 nm; λ_{em}, 312, 356, 377 nm and Φ_s= 0.33. The positions of emission bands remain unchanged when λ_{ex} is varied between (λ_{ex} - 10) and (λ_{ex} + 10) nm.

Catechol oxidase studies of complexes

Catalytic oxidation of 3,5-di-*tert*-butylcatechol (3,5-DTBC) to 3,5-di-*tert*-butylquinone (3,5-DTBQ) was carried out based on the following reaction,[34] where complexes **1-3** were used as catalyst.

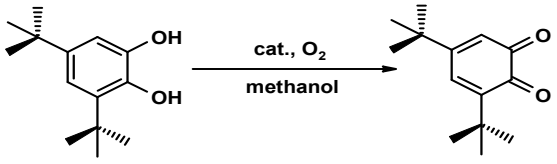

3,5-DTBC **3,5-DTBQ**

RSC Advances Accepted Manuscript

Catecholase activities of **1-3** were tested by adding their 1 x 10^{-4} M methanolic solution to a 1 x 10^{-2} M solution of 3,5-DTBC at 30 °C under aerobic condition and the progress of the reaction were studied based on the UV-vis spectra of the mixture at five minute interval for up to 90 min. A band at 400 nm corresponding to 3,5-DTBQ was gradually increased (Figs. 9, 23S and 24S) after addition of complex to the solution of 3,5-DTBC.[35] Kinetics of the oxidation of 3,5-DTBC were determined by examining the growth of the 3,5-DTBQ band at 400 nm as function of time (t).[34] From the $\log \frac{A_\infty}{(A_\infty - A_t)}$ versus time (t) plot (Fig. 10) (where A_∞ and A_t are the absorbance at infinite time and at t time, respectively, corresponding to the band at 400 nm), the rate constants for complex-substrate mixtures were determined and the calculated values were 1.33 x 10^{-2} min^{-1}, 1.78 x 10^{-2} $min^{-1}$and 1.42 x 10^{-2} min^{-1} for **1**, **2** and **3**, respectively. Different rate of catalytic activities of **1-3** may be explained by considering their geometries. The compound having more distorted square pyramidal (*SPY*-5) geometry shows higher rate of catalytic activity. Trigonality τ parameters (*vide supra*) indicate the order of deviation from regular geometries as **2** > **3** > **1**, which corroborate the order of rate of catalytic reactions.

We have added the solution of complexes to the various concentration of 3, 5-DTBC (from 1 x 10^{-3} M to 10 x 10^{-3} M) under aerobic condition to realize the dependence of the reaction rate on substrate concentration. But we did not observe saturation kinetics even at higher concentration of 3, 5-DTBC (Fig. 25S). ESI MS spectral studies of solution containing complexes and 3, 5-DTBC were performed to establish the possible mechanism. Unfortunately we were unable to characterize the intermediates. However, when a mixture of starch-potassium iodide solution was added to a mixture of complex and 3, 5-DTBC, blue coloration developed, which indicates that hydrogen peroxide was produced during the course of reaction. It is interesting to note that no blue coloration was observed in absence of 3,5-DTBC. Possible

RSC Advances Accepted Manuscript

mechanistic path of the formation of H_2O_2 as by-product during the oxidation of 3,5-DTBC to 3,5-DTBQ catalyzed by copper(II) compound was suggested by Chyn and Urbach.[36] Considering the formation of hydrogen peroxide during the reaction we have proposed a probable mechanism (Scheme 1S, supporting information), where catalytic reaction started with the formation of intermediate I, where two copper complexes are bridged by 3,5-DTBC. Copper complexes then gain one electron each from 3,5-DTBC and from intermediate II, where two reduced copper compounds are bridged with 3,5-DTBQ. Molecular oxygen then oxidizes complexes and form peroxide (O_2^{2-}) bridged intermediate III. In presence of proton, H_2O_2 and 3,5-DTBQ are liberated and complexes are regenerated.

Cytotoxicity assay

The antiproliferative activity of the complexes was tested by standard MTT assay using MCF7 cells. All the complexes show dose dependent suppression of cell viability (Fig. 26S).[37] The half maximal inhibitory concentration (IC_{50}) values of complexes are 30 ± 2.7 μM, 68 ± 6.6 μM, and >100 μM for complexes **1**, **2** and **3**, respectively. Results reveal that complex **1** has more potent cytotoxic effect on breast cancer cell line MCF7 as compared to complexes **2** and **3**. More cytotoxic effect of **1** probably due to its smaller size, which favors its incorporation to the active site of the cancer cell and destroys the cancer cells easily. On the other hand the presence of nonpolar group in the R2 position suppresses the anti-proliferative effect of compound **3**. Anticancer activities of **1-3** have been compared (Fig. 11) with the anticancer activity of cisplatin on breast cancer cell line MCF7 and result shows that complexes **1-3** are less efficient than cisplatin (Table 6).

RSC Advances Accepted Manuscript

Conclusion

We have presented here the synthesis, characterization and photophysical studies of three N,N,N,O donor tetradentate ligands. The geometry optimization of the ligands shows that two ligands are stable in their ketotautomeric form whereas other ligand has comparable stability in keto and enol tautomeric forms in the ground state. Three square pyramidal Cu(II) complexes have been synthesized using these ligands and in the solid state all the complexes are stabilized by weak interactions. The DFT computations of the isolated complexes are in good agreement with the structural results obtained by X-ray diffraction. Results of TD-DFT calculations have been discussed in term of theoretically possible spin allowed doublet-doublet electronic transitions along with their assignments. The influence of different functionals used in geometry optimization and excite state TD-DFT calculations of complexes reveals that among the B3LYP, B3PW91 and MPW1PW91 functionals, B3LYP was able to best reproduce the experimental results. Complexes **1-3** are active in catalyzing the aerobic oxidation of 3,5-DTBC to 3,5-DTBQ and catalytic activity increases with increasing distortion in geometries of complexes. Cytotoxic activity of the complexes towards human breast (MCF7) cancer cell lines follow the order of **1** > **2** > **3**, and cytotoxic effect of **1-3** are relatively low compare to cytotoxic effect of cisplatin.

Acknowledgements

The authors gratefully acknowledge the financial assistance given by the CSIR, Government of India, to Dr. Subal Chandra Manna (Project No. 01 (2743)/13/EMR-II). M. K. S thankful to DBT, Govt. of India, for Ramalingaswami fellowship.

RSC Advances Accepted Manuscript

Supplementary information

X-ray crystallographic data in CIF format, Details of synthesis of ligands, IR spectra, Figs. of electronic spectra and results of DFT/TDDFT calculation of HL^1, HL^2, HL^3 and complexes **1-3** are provided as supplementary material.

References

(1) M. G. Gichinga and S. Striegler, *J. Am. Chem. Soc.* 2008, **130**, 5150.

(2) M. Barwiolek, E. Szlyk, A. Berg, A. Wojtczak, T. Muziol and J. Jezierska, *Dalton Trans.* 2014, **43**, 9924.

(3) K. Dhara, U. C. Saha, A. Dan, S. Sarkar, M. Manassero and P. Chattopadhyay, *Chem. Commun*., 2010, **46**, 1754.

(4) P. Kumar, S. Gorai, M. K. Santra, B. Mondal and D. Manna, *Dalton Trans.* 2012, **41**, 7573.

(5) (a) B. Duff, V. R. Thangella, B. S. Creaven, M.; Walsh and D. A. Egan *Eur. J. Pharma.* 2012, **689**, 45; (b) A. T. Chaviara, P. C. Christidis, A. Papageorgiou, E. Chrysogelou, D. J. Hadjipavlou-Litina and C. A. Bolos*, J. Inorg. Biochemistry* 2005, **99**, 2102.

(6) K. S. Banu, T. Chattopadhyay, A. Banerjee, S. Bhattacharya, E. Suresh, M. Nethaji, E. Zangrando and D. Das, *Inorg. Chem.* 2008, **47**, 7083.

(7) M. S. Ray, S. Chattopadhyay, M. G. B. Drew, A. Figuerola, J. Ribas, C. Diaz and A. Ghosh, *Eur. J. Inorg. Chem.* 2005, 4562.

(8) (a) B. Sarkar, S. Konar, C. J. G. mez-García and A. Ghosh, *Inorg. Chem.* 2008, **47**, 11611; (b) B. Sarkar, M. S. Ray, Y.-Z. Li, Y. Song, A. Figuerola, E. Ruiz, J. Cirera, J. Cano and A. Ghosh, *Chem. Eur. J.* 2007, **13**, 9297.

RSC Advances Accepted Manuscript

(9) (a) M. K. Casida, D. P. Chong (Eds.), Rescent Advances in Density Functional Methods, Part I, World Scientific, Singapore, 1995; (b) R. E. Stratmann, G. E. Scuseria and M. J. Frisch, *J. Chem. Phys.* 1998, **109**, 8218.

(10) (a) C. Lee, W. Yang and R. G. Parr, *Phys. Rev.* 1988, **37 B**, 785; (b) H. Ihee, J. Kua, W. A. Goddard III, A. H. Zewail, *J. Phys. Chem. A,* 2001, **105***,* 3623; (c) J. P. Safko, J. E. Kuperstock, S. M. McCullough, A. M. Noviello, X. Li, J. P. Killarney, C. Murphy, H. H. Patterson, C. A. Bayse, R. D. Pike, *Dalton Trans.*, 2012, **41**, 11663.

(11) (a) S. Mistri, S. García-Granda, E. Zangrando and S. C. Manna, *Polyhedron*, 2013, **50**, 333; (b) S. Mistri, E. Zangrando and S. C. Manna, *Inorganica Chimica Acta*, 2013, **405**, 331.

(12) D. D. Perrin, W. L. F. Armarego, D. R. Perrin, Purification of Laboratory Chemicals; Pergamon Press: Oxford, U.K., 1980.

(13) J. R. Lakowicz, Principles of Fluorescence Spectroscopy, Third Edition, Springer, New York, USA, 2006.

(14) Z. Otwinowski, W. Minor, Methods in Enzymology, C.W. Carter, R.M. Sweet Editors, Part A, Academic Press, London, 1997, **276**, 307.

(15) R. H. Blessing, *Acta Crystallogr. Sect A,* 1995, **51**, 33.

(16) A. Altomare, M. C. Burla, M. Camalli, G. L. Cascarano, C. Giacovazzo, A. Guagliardi, A. G. Moliterni, G. Polidori and R. Spagna, *J. Appl. Crystallogr.* 1999, **32**, 115.

(17) G. M. Sheldrick, SHELX-97, Program for Crystal Structure Refinement, University of Gottingen, Germany, 1997.

(18) M. Nardelli, *J. Appl. Crystallogr.* 1995, **28**, 659.

(19) L. J. Farrugia, *J. Appl. Crystallogr.* 1999, **32**, 837.

RSC Advances Accepted Manuscript

(20) K. Brandenburg, DIAMOND (Version 3.2i), Crystal Impact GbR, Bonn, Germany (1999).

(21) Gaussian 09, revision A.02; Gaussian, Inc.: Wallingford, CT, 2009.

(22) P. J. Hay and W. R. Wadt, *J. Chem. Phys.* 1985, **82**, 270.

(23) (a) A. Douhal, F. Lahmani and A. Zewail, *Chem. Phys.* 1996, **207**, 477; (b) J. Catalan and J. L. P. De Paz, *J. Phys. Chem A.* 2001, **105**, 7315.

(24) (a) R. E. Stratmann, G. E. Scuseria and M. J. Frisch, *J. Chem. Phys.* 1998, **109**, 8218; (b) M. E. Casida, C. Jamorski, K. C. Casida and D. R. Salahub, *J. Chem. Phys.* 1998, **108**, 4439.

(25) M. Cossi, N. Rega, G. Scalmani and V. Barone, *J. Comput. Chem.* 2003, **24**, 669.

(26) N. M. O'Boyle, A. L. Tenderholt and K. M. Langner, *J. Comput. Chem.* 2008, **29**, 839.

(27) M. N. Burnett and C. K. Johnson, ORTEP III, Report ORNL-6895, Oak Ridge National Laboratory, Oak Ridge, TN, 1996.

(28) M. C. Etter and J. C. MacDonald Bernstein, *J. Acta Crystallogr.* 1990, **B46**, 256.

(29) M. Nishio, M. Hirota and Y. Umezawa, The C−H···π Interaction: Evidence, Nature and Consequences, Wiley-VCH, New York, 1998.

(30) D. Cremer and J.A. Pople, *J. Am. Chem. Soc*. 1975, **97**, 1354.

(31) (a) H.-L. Zhu, S.-Y. Li, Z.-D. Wang and F. Yang, *J. Chem Crystallogr.* 2004, **34**, 203; (b) F. Cusmano Priolo, E. Rotondo, G. Rizzardi, G. Bruno and G. Bombieri, *Acta Cryst*., 1983, **C39**, 550.

(32) J. Aihara, *J. Phys. Chem. A*, 1999, **103**, 7487.

(33) A.W. Addison, T.N. Rao, J. Reedijk, J.V. Rijn and G. C. Verschoor, *J. Chem. Soc. Dalton Trans.* 1984, 1349.

(34) (a) P. Seth, L. K. Das, M. G. B. Drew and A. Ghosh, *Eur. J. Inorg. Chem.* 2012, 2232; (b) P. Kar, R. Haldar, C. J. Gómez-García and A. Ghosh, *Inorg. Chem.* 2012, **51**, 4265.

RSC Advances Accepted Manuscript

(35) (a) F. Zippel, F. Ahlers, R. Werner, W. Haase, H.-F. Nolting and B. Krebs, *Inorg. Chem.* 1996, **35**, 3409; (b) A. Biswas, L. K. Das, M. G. B. Drew, C. Diaz and A. Ghosh, *Inorg. Chem.* 2012, **51**,10111.

(36) J.-P. Chyn and F. L.Urbach, *Inorg. Chim. Acta*, 1991, **189**, 157.

(37) L. Tavares, S. Johann, T. Alves, J. Guerra, E. Souza-Fagundes, P. Cisalpino, A. J. Bortoluzzi, G. F. Caramori, R. Piccoli, H. T.S. Braibante, M. E.F. Braibante, M. G. Pizzolatti, *Eur. J. Med. Chem*. 2011, **46**, 4448.

RSC Advances Accepted Manuscript

Table 1. Crystal data and structure refinement for complexes **1** - **3**.

Complex	**1**	**2**	**3**
Empirical formula	$C_{11}H_{18}CuClN_3O_6$	$C_{12}H_{20}CuClN_3O_7$	$C_{12}H_{20}CuClN_3O_6$
Formula mass (g mol^{-1})	387.27	417.30	401.30
Space group	P21/c	P3121	P21/c
Crystal system	Monoclinic	Trigonal	Monoclinic
a (Å)	9.9206(3)	12.3073(5)	10.0150(10)
b (Å)	14.4822(4)	12.3073(5)	14.9210(10)
c (Å)	10.9734(3)	19.1117(6)	11.0160(10)
α (°)	90	90	90
β (°)	100.5371(15)	90	107.720(10)
γ (°)	90	120	90
V (Å^3)	1549.98(8)	2507.01(16)	1568.1(3)
Z	4	6	4
T (K)	295	295	295
D_{calc} (g cm^{-3})	1.660	1.658	1.700
F(000)	796	1290	828
μ (Mo-Kα) (cm^{-1})	16.13	15.07	15.97
Meas. refl.	6745	6036	12909
Unique refl.	3721	3265	3063
R_{int}	0.0192	0.029	0.0338
Obs. refl. [I≥2σ(I)]	3074	2732	2324
θ_{min}- θ_{max} / °	3.78-28.00	3.8-26.00	2.13-26.00
hkl ranges	-13, 13; -19, 17; -14, 14	-15,15; -12, 12; -22, 23	-12, 9; -18,18; -13, 13
R1 [I≥2σ(I)][a]	0.0424	0.0420	0.0472
*w*R2 [I≥2σ(I)][a]	0.1223	0.1080	0.1409
No. Variables/ Constraints	219/5	238/5	229/5
Goodness of fit	1.046	1.030	1.051
Δρ max; Δρ min (e Å^{-3})	0.745; -0.452	0.43; -0.44	0.999; -0.574

[a] $R1(Fo) = \Sigma \left| \left| Fo \right| - \left| Fc \right| \right| / \Sigma \left| Fo \right|$, $wR2(Fo^2) = [\Sigma w (Fo^2 - Fc^2)^2 / \Sigma w (Fo^2)^2]^{1/2}$

RSC Advances Accepted Manuscript

Table 2. Experimental and calculated[b] coordination bond lengths (Å) and angles (°) for complexes **1-3**.

Complex	**1**		**2**		**3**	
	Exp	Calcd	Exp	Calcd	Exp	Calcd
Bond lengths						
Cu1- O1	1.922(2)	1.940	1.908(3)	1.940	1.862(3)	1.911
Cu1-O2	2.394(2)	2.328	2.428(3)	2.330	2.465(3)	2.353
Cu1- N1	1.939(2)	1.977	1.935(6)	1.973	1.924(3)	1.994
Cu1 -N2	2.009(2)	2.061	2.029(4)	2.060	1.960(3)	2.041
Cu1 -N3	2.010(3)	2.065	1.988(5)	2.062	2.029(4)	2.073
Bond angles						
O1 -Cu1-O2	96.40(1)	100.86	90.22(12)	100.71	94.90(1)	100.54
O1-Cu1-N1	94.20(1)	93.62	94.61(18)	93.39	89.00(1)	93.72
O1 -Cu1-N2	172.90(1)	172.83	178.26(14)	173.09	176.80(2)	173.45
O1 -Cu1-N3	95.00(1)	94.71	96.02(18)	94.85	99.50(1)	93.60
O2 -Cu1-N1	101.80(1)	98.50	107.66(14)	98.64	102.30(1)	96.13
O2 -Cu1-N2	90.70(1)	86.28	88.40(14)	86.15	88.10(1)	85.94
O2 -Cu1-N3	89.10(1)	96.28	90.94(15)	96.25	88.40(2	96.52
N1 -Cu1-N2	84.60(1)	84.71	84.80(2)	84.81	91.40(2)	86.33
N1-Cu1 -N3	164.90(1)	161.32	158.52(17)	161.30	165.80(2)	163.95
N2 -Cu1-N3	84.70(1)	84.94	85.10(2)	84.98	79.50(2)	84.77
τ_5 parameter[33]	0.133	0.191	0.329	0.196	0.183	0.158

[b] Using conductor-like polarizable continuum model (CPCM) in methanol; basis set, LanL2DZ; B3LYP functional.

Table 3. Ring conformations: Puckering parameters for complexes **1-3**.

Complex	**Ring 1** (Cu1,N1,C8,C9,N2)			**Ring 2** (Cu1,N2,C10,C11,N3)		
	q_2/Å	φ2/◦	Conformation	q_2/Å	φ_2/◦	Conformation
1	0.415(3)	106.8(3)	Envelope: E_4	0.431(3)	-101.0(4)	Twisted/Envelope : $^4T_3/E_3$
2	0.406(4)	120.0(6)	Twisted/Envelope: $^5T_4/E_4$	0.410(5)	-79.0(5)	Twisted/Envelope : $^4T_3/^4E$
3	0.403(5)	101.6(5)	Twisted/Envelope: $^3T_4/E_4$	0.425(5)	-105.4	Envelope: E_3

RSC Advances Accepted Manuscript

Table 4. Selected UV-vis energy transition at the TD-DFT/B3LYP level for **1, 2** and **3** in methanol.

Complex	Excited state	λ_{cal} (nm), ε_{cal} ($M^{-1}cm^{-1}$), (eV)	Oscillator strength (f)	λ_{exp} (nm), ε_{exp} (M^{-1} cm^{-1}), (eV)	Key transition	Character[c]
1	D_8	364.07,4512, (3.40)	0.0508	361, 7217, (3.43)	HOMO -1(α) →LUMO (α) (11%), HOMO (α) →LUMO (α) (36%), HOMO (β) →LUMO+1(β) (36%)	$ILCT^{\theta}$ $ILCT^{\theta}$ $ILCT^{\theta}$
	D_9	359.35, 4557, (3.45)	0.0097		HOMO -1(α) →LUMO (α) (81%)	$ILCT^{\theta}$
	D_{15}	260.20, 27361, (4.76)	0.2766	267, 22565, (4.64)	HOMO -2(α) →LUMO (α) (20%), HOMO -4(β) →LUMO (β) (12%), HOMO -1(β) →LUMO+1(β) (17%)	$ILCT^{\theta}$ $LMCT^{\delta}$ $ILCT^{\theta}$
	D_{19}	243.92, 18615, (5.08)	0.0455	241.50, 29043, (5.13)	HOMO (α) →LUMO+1(α) (19%), HOMO -7(β) →LUMO (β) (18%)	$ILCT^{\theta}$ $LMCT^{\delta}$
	D_{31}	222.10, 7183, (5.58)	0.0003	224, 27086, (5.53)	HOMO-1(α) →LUMO+1(α) (10%), HOMO -1(α) →LUMO+2(α) (82%)	$ILCT^{\theta}$ $LMCT^{\delta}$
	D_{41}	204.90, 18843, (6.05)	0.0015	205, 13434, (6.04)	HOMO (β) →LUMO+7(β) (43%)	$LMCT^{\delta}$
	D_{42}	204.46,18661,(6.06)	0.0017		HOMO -2(β) →LUMO+2(β) (50%), HOMO (β) →LUMO+7(β) (13%)	$ILCT^{\theta}$ $LMCT^{\delta}$
2	D_9	373.06, 3778, (3.32)	0.0063	375, 4242, (3.30)	HOMO -1(β) → LUMO (β) (69%)	$LMCT^{\Gamma}$
	D_{27}	232.29, 21528, (5.33)	0.1648	236.50, 27333, (5.24)	HOMO (α) →LUMO +2(α) (28%), HOMO (β) →LUMO+3(β) (24%)	$ILCT^{\psi}$ $ILCT^{\psi}$
	D_{45}	206.87, 11734, (5.99)	0.0263	206, 19727, (6.01)	HOMO-2(α) →LUMO+1 (α) (17%), HOMO -1(β) →LUMO+2(β) (43%)	$LMCT^{\Gamma}$ $LMCT^{\Gamma}$
3	D_9	353.62, 5498, (3.50)	0.0247	355, 3125, (3.49)	HOMO-1(α) → LUMO (α)(70%)	$ILCT^{\Phi}$
	D_{27}	230.04, 11542, (5.38)	0.0047	224.50, 21812, (5.52)	HOMO-1(α) → LUMO+1(α)(51%), HOMO -1(α) →LUMO+2(α) (14%)	$LMCT^{\Omega}$ $ILCT^{\Phi}$
	D_{42}	206.36, 6460, (6.00)	0.0189	204.50, 27625, (6.06)	HOMO (α) →LUMO+6(α) (46%), HOMO (β) →LUMO+7(β) (26%)	$LMCT^{\Omega}$ $LMCT^{\Omega}$
	D_{44}	202.09, 1491, (6.13)	0.0018		HOMO-1(α) →LUMO+4(α) (46%)	$LMCT^{\Omega}$

[c] $ILCT^{\theta}$ = intra ligand charge transfer transition in L^1; $ILCT^{\psi}$ = intra ligand charge transfer transition in L^2; $ILCT^{\Phi}$ = intra ligand charge transfer transition in L^3; $LMCT^{\delta}$ = L^1 to metal charge transfer transition; $LMCT^{\Gamma}$ = L^2 to metal charge transfer transition and $LMCT^{\Omega}$ = L^3 to metal charge transfer transition.

Table 5. Photophysical parameters of complexes **1**, **2** and **3**.

Complex	λ_{ex}(nm), ε_{exp} ($M^{-1}cm^{-1}$), (eV)	λ_{em}(nm)	Δν [d] (nm)	φ
1	267, 22478, (4.64)	312, 329, 357	45, 62, 90	0.52
2	272, 16455, (4.56)	312, 329, 355	40, 57, 83	0.46
3	266, 11312, (4.67)	312, 356, 377	47, 91, 112	0.33

[d]Stoke shift

RSC Advances Accepted Manuscript

Table 6. Anticancer activity of complexes **1-3** and cisplatin against breast cancer cell line MCF7.

Compound	**1**	**2**	**3**	**cisplatin**
IC50 (μM)	31.07 ± 6.67	42.63 ± 7.13	>100	6.83 ± 1.40

Caption of the Figures

Fig. 1. ^{1}H NMR spectra of **HL^{1}**, **HL^{2}** and **HL^{3}** in $CDCl_3$.

Fig. 2. ORTEP diagram (ellipsoids at 30% probability) of **1**.

Fig. 3. Supramolecular dimeric assembly of **1**.

Fig. 4. Supramolecular trimeric assembly of **2**.

Fig. 5. Supramolecular dimeric assembly of **3**.

Fig. 6. Potential energy curve at the ground S_0 state for HL^1 calculated at the DFT/B3LYP level.

Fig. 7. Theoretical (red line) and experimental (black line) electronic spectra (left) of **1**. The most prominent MOs involving transitions (right) and their diagrams.

Fig. 8. Fluorescence spectra of complexes [for **1**, red line, λ_{ex} = 267 nm; for **2**, green line, λ_{ex} = 272 nm; for **3**, blue line, λ_{ex} = 265 nm; excitation and emission slit width = 2.5 nm].

Fig. 9. Increase in the 3,5-di-*tert*-butylquinone (3,5-DTBQ) band at 400 nm after addition of 10^{-4} M methanolic solution of complex **1** to 100 fold methanolic solution of 3,5-DTBC. The spectra were recorded at an interval of 5 min.

Fig. 10. Change in absorption maxima at 400 nm with time after addition of 10^{-4} M methanolic solution of complex to 100 fold methanolic solution of 3,5-DTBC**.** Circle (**1**), square (**2**) and triangle (**3**).

RSC Advances Accepted Manuscript

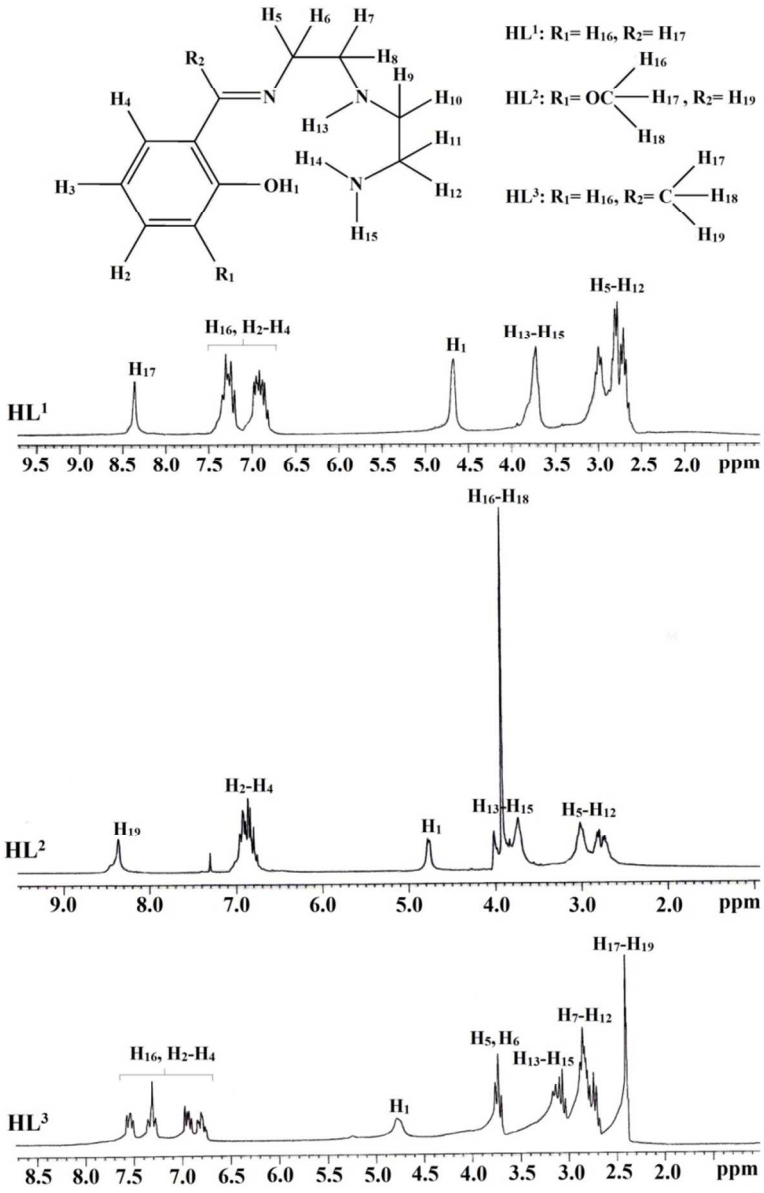

Fig. 1

RSC Advances Accepted Manuscript

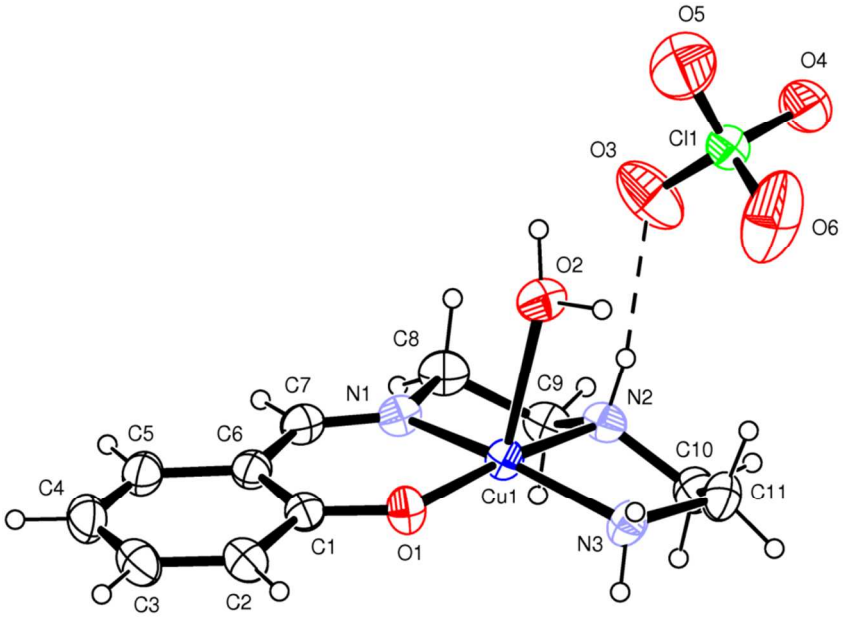

Fig. 2

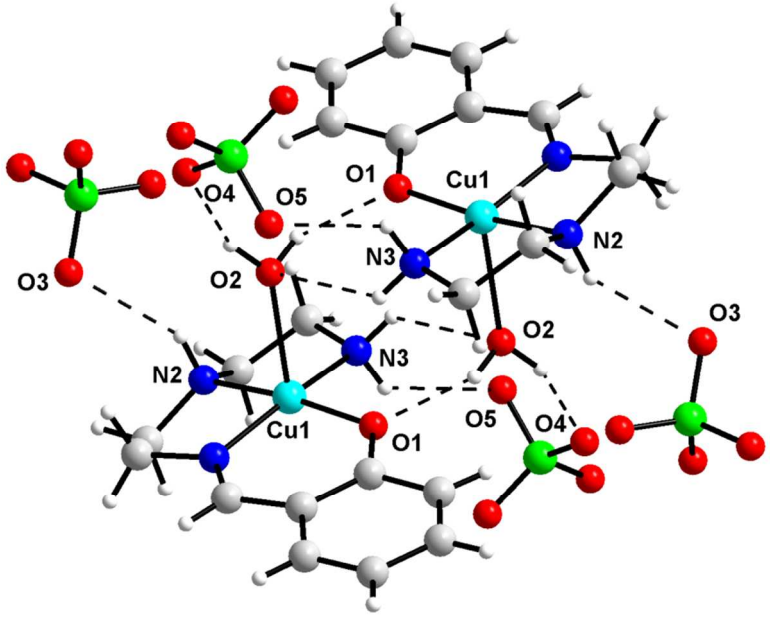

Fig. 3

RSC Advances Accepted Manuscript

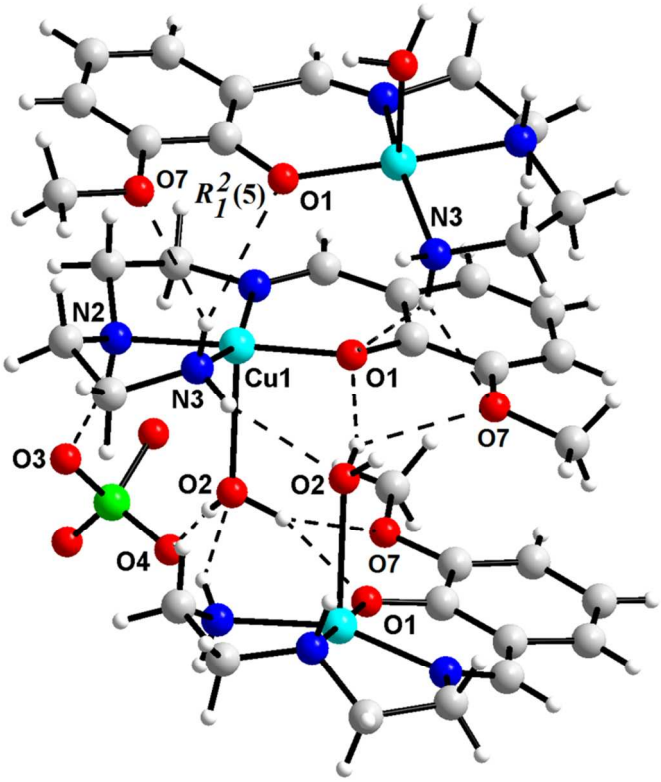

Fig. 4

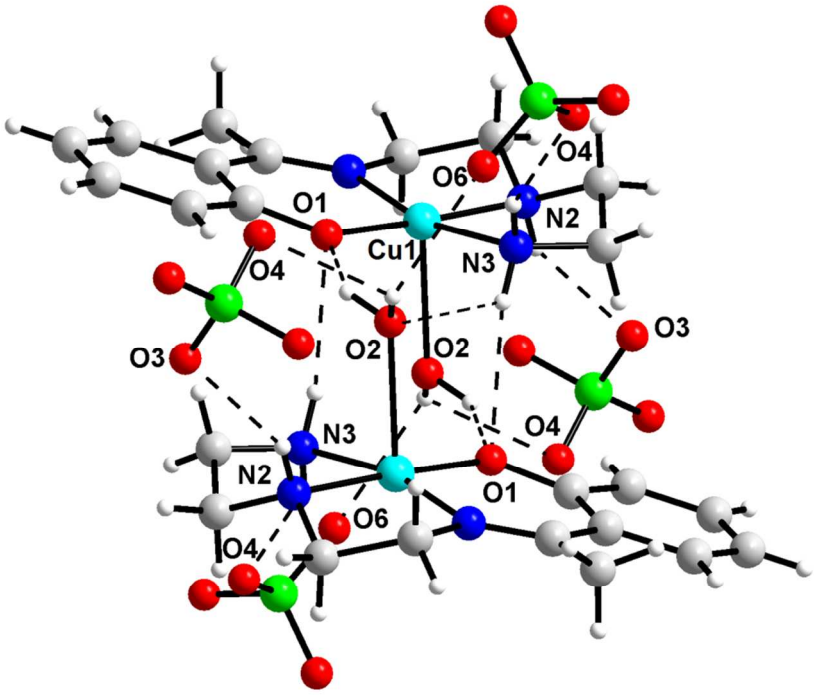

Fig. 5

RSC Advances Accepted Manuscript

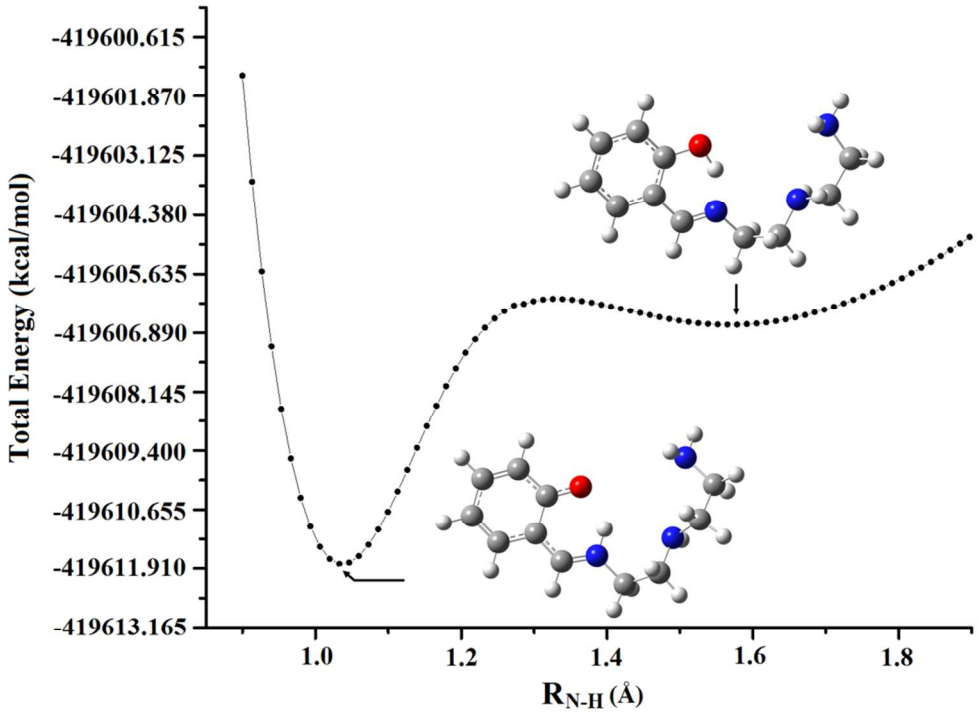

Fig. 6

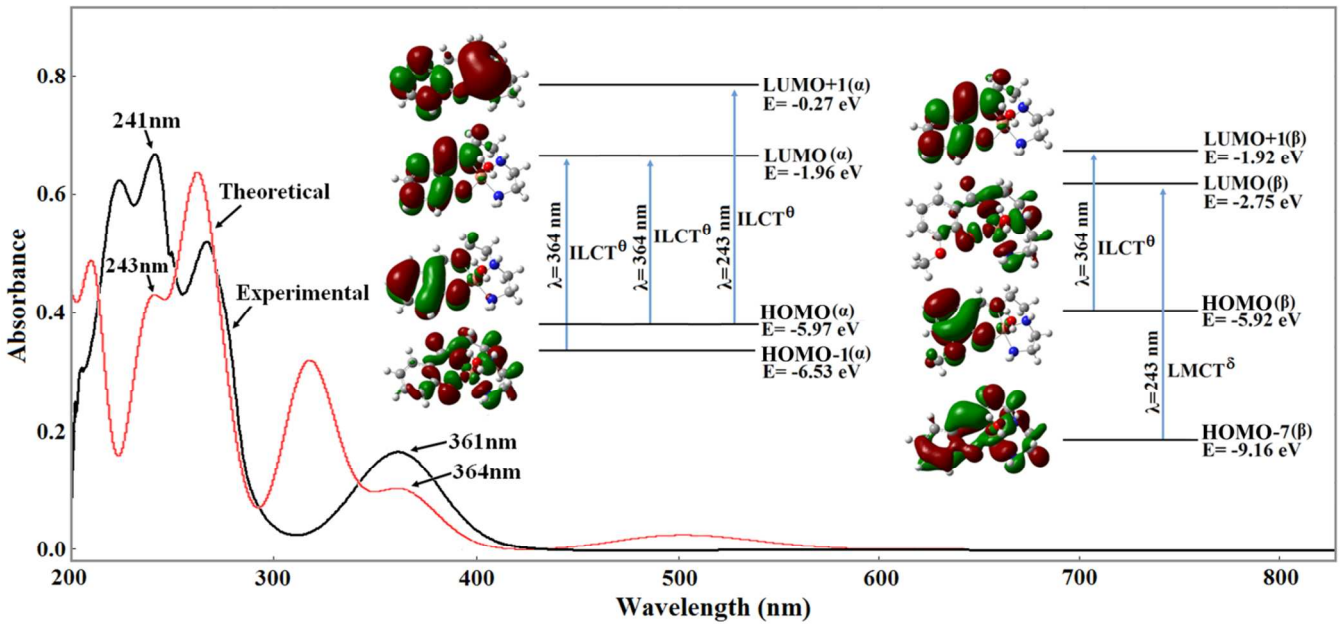

Fig. 7

RSC Advances Accepted Manuscript

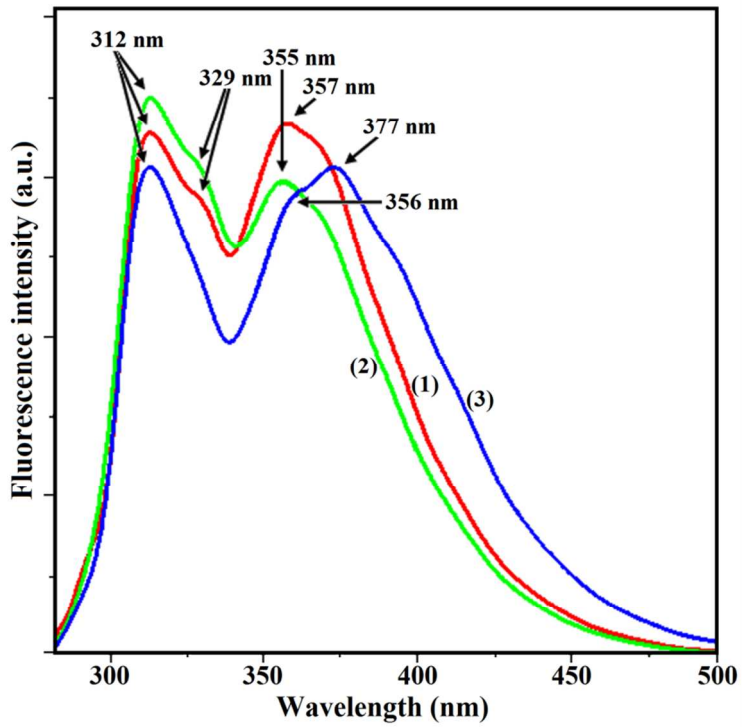

Fig. 8

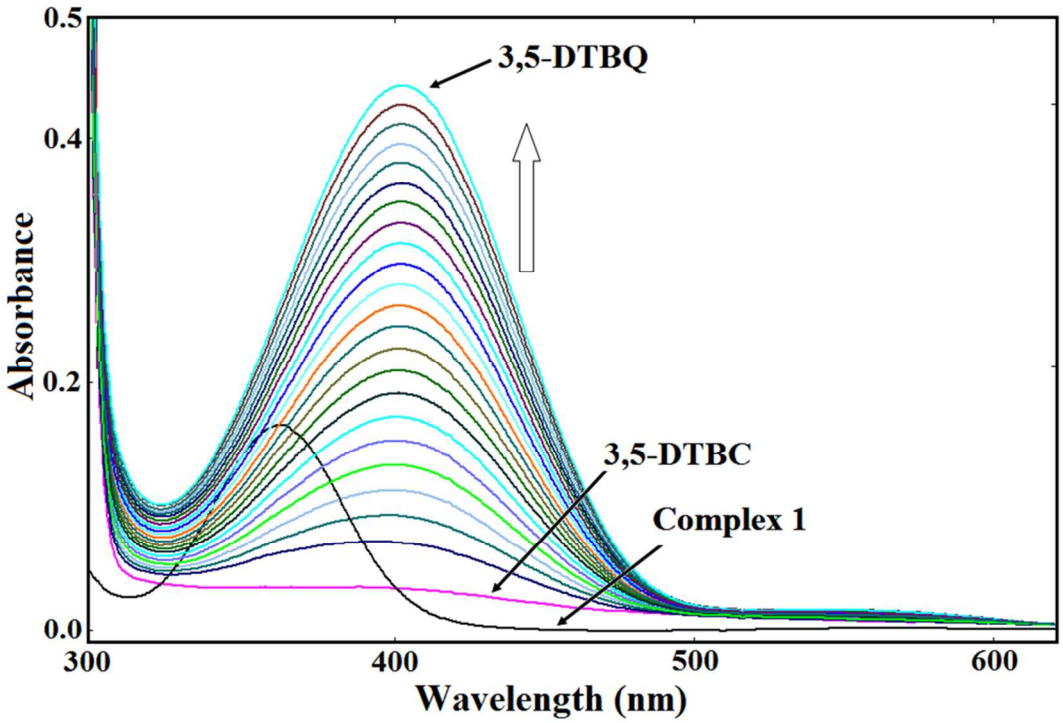

Fig. 9

RSC Advances Accepted Manuscript

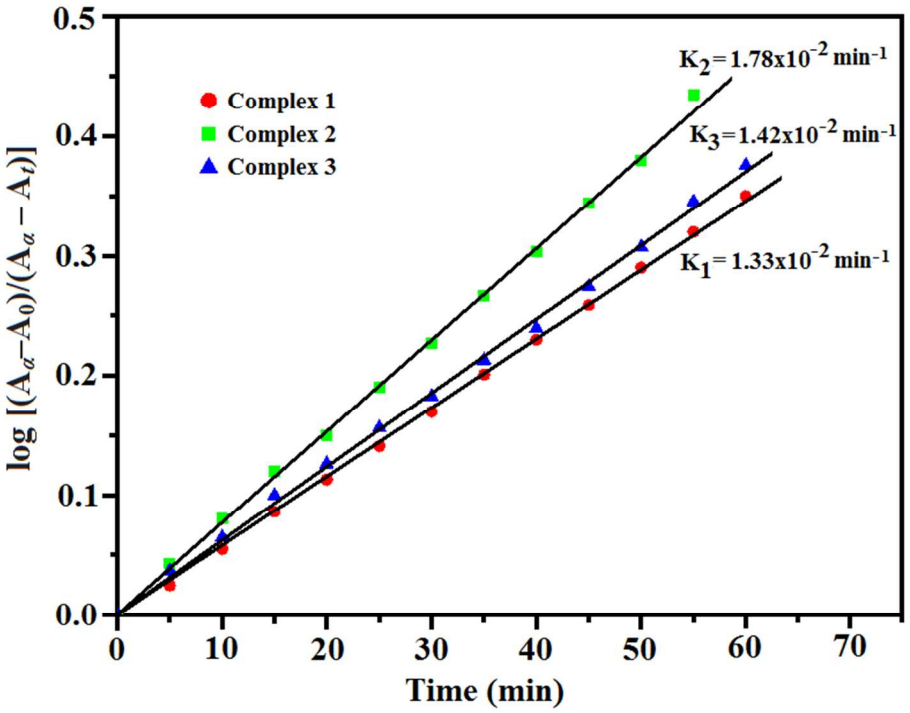

Fig. 10

RSC Advances Accepted Manuscript